The Control of a Mobile Robot based on a Scalar-valued Signal Field gathered by Airflow Sensor Measurements

Author: Titus Kraanen *Supervisors:* Bayu Jayawardhana Mauricio Muñoz Arias

***Abstract* – Flow measurements can enable an autonomous mobile robot to master its environment. In this report a designed control law is presented. The control law enables the autonomous mobile robot to locate and follow the path where the strength of the scalar field is the lowest. The gradient descent algorithm is used to solve the conditions the control law requires, where the gradient information is solely provided by flow sensors. Monte Carlo simulations are executed to validate the control law. The simulations are performed under different circumstances (e.g. varying in gains of constant values).**

I. INTRODUCTION

The developments in the world of robotics and autonomous vehicles have led to the establishment of the fourth industrial revolution [1]. Autonomous control systems for vehicles is one of the disruptive technologies. Currently, the autonomous vehicles use different types of sensors as input to navigate themselves. Olfactory sensors can be used to detect and follow odour trails [2]. Optical sensors are able to determine where the vehicle is located based on recordings [3]. Next, ultrasonic sensors can executed precise distances measurement to navigate a vehicle [4]. In this project airflow sensors will be used to control the autonomous vehicle. Flow sensors can measure the volumetric rate, velocity, pressure, and shear stress of its surroundings [5].

Over the past years, the traffic intensity is escalating [6]. The demand is for freight transportation is expected to increase in the coming years [7]. Simultaneously, these transportations of goods cause CO_2 emissions. The transport sector is roughly accountable for 21% of the CO_2 emissions in the European Union. The freight transportation is responsible for about a quarter of these emissions [7].

In the system of road transport, following the trajectory where the airflow is measured the lowest can be a crucial aspect in reducing the CO_2 emissions. The overall aerodynamic drag is lowered when, for example, a truck follows the path where the airflow related to the truck is the lowest [6], [8]. Consequently, the fuel consumption and CO_2 emissions reduce.

In the scope of this report, the origin is an airflow field, where the airflow sensor measurements enable the autonomous mobile to understand its environment. The airflow sensors assist the control system to steer the mobile robot towards the right trajectory.

The airflow sensors gather data of the surroundings of the mobile robot. The data consist of scalar-valued field, where every position in the field includes its own magnitude (i.e. the scalar value or gradient vector). Based on the data, a signal is provided to control system, which steers the mobile robot to the right trajectory.

The gradient vector information is needed to compute control algorithm for the mobile robot. In this report, the gradient-descent algorithm is deployed to provide to right signal to the control system. Controlling a vehicle by the gradient-ascent/descent algorithm is an acknowledge way to control a mobile robot in an unknown environment [9], [10], [11]. The convex combination for the approximation of the gradient is introduced, when there is a lack of information about the gradient vector in the signal field.

The contribution of this report is the proposition of a design of a control system based on local gradient information, that is obtained from a scalar-valued field corresponding with a flow. The control law is arranged with the gradient-ascent/descent algorithm. The angular velocity of the mobile robot is controlled by this control law. The forward velocity is set as constant in this report.

The report is structured as follows. In Section II the problem is described and the conditions and aim of the control system is discussed. Section III present the system and explanations about kinematics of the mobile robot, the scalar field, gradient and convex combination. Next, the design of the control law is presented in this section. In Section IV the simulations are executed and the results are shown. In the last two Section V and VI, the results are discussed and a conclusion is provided.

II. PROBLEM DISCRIPTION

The aim of the autonomous mobile robot is to follow the trajectory where magnitude of the scalar value on the field is the lowest. To achieve this aim, the robot must seek the minimum scalar value in the signal field. Besides, the mobile robot must be capable to follow the path where the scalar value, corresponding with the airflow, is the lowest.

A. Environments

The mobile robot must be able to understand its environment with solely the help of the airflow sensors and the designed control law. In the scope of this report, the environment is set to two different scalar-valued signal fields. These airflow fields are analyzed and simulated in Section IV. The scalar and gradient fields are depicted in Figure 1 and 2 and described as follows.

The unknown nonlinear map $J(x,y)$ has a minimum where $J(x,y) = 0$. The signal field $J(x,y)$ is defined as follows,

$$J(x,y) = \text{dist}\left(\begin{bmatrix} x \\ y \end{bmatrix}, \Omega\right) \quad (1)$$

where Ω is the level set given by, $\{(x,y)|y = f(x)\}$ or $\{(x,y)|x = f(y)\}$.

The two unknown nonlinear maps J_1 and J_2 are defined as follows,

$$J_1(x,y) = J_1(f(y),y) \quad (2)$$

$$J_2(x,y) = J_2(x,f(x)) \quad (3)$$

where $f(y) = 0$ and $f(x) = 0.01x^3$

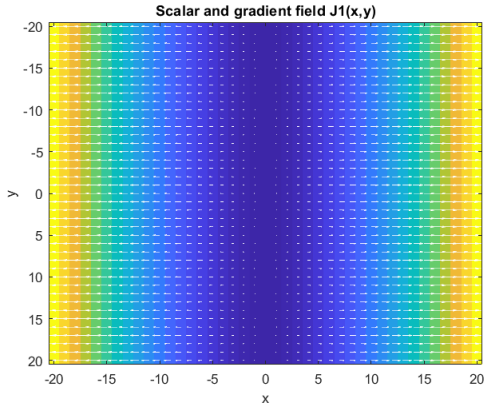

Figure 1: Scalar field and gradient field of $J_1(x,y)$

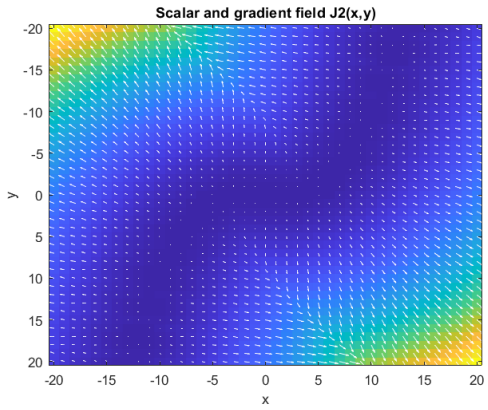

Figure 2: Scalar field and gradient field $J_2(x,y)$

The mobile robot is placed randomly in an environment where an unknown signal is applied. This signal field is shown in Figure 1 and 2. The colors corresponds with the scalar value. The longer the distance from a given point to the function, the higher the scalar value (e.g. the distance is zero when the point is located on the function and corresponds with the dark blue color). The distribution of the increase or decrease of the scalar field is characterized by the gradient. The gradient is a vector field that represents the direction and rate of the fastest increase at a given point. The direction of the vector shows the direction in which the scalar field rises most (i.e. the white arrows). The magnitude of this vector is equal to the rate of increase in that direction. The direction of the vectors in Figure 1 and 2 correspond to the increase of scalar value. The mobile robot only measures the value of the gradient at its real-time location. Based on this information it tries to steer to the local minimum. Consequently, the location of the robot depends on its previous location only.

III. CONTROL SYSTEM

A. *System*

As mentioned in the problem description, the autonomous mobile robot aims to search for and navigate towards the minimum of a scalar signal field. The robot is placed in an environment where an unknown nonlinear signal field is applied. The scalar-valued function defines the signal, which represents the airflow coming from all possible directions. This unknown signal field contains a path where the airflow is minimized to zero.

The control system of the mobile robot is explained in Figure 3. The controller in the system provides the values of the forward and angular velocity to the robot. The specific control law will be discussed in Section III.F.

In this system the value of the forward velocity v is set as a constant. The angular velocity u of the mobile robot determines the next real-time location and should steer the robot to the local minimum. To determine the value of the angular velocity u the gradient (∇J) is needed. The sensors on the mobile robot measure the local gradient in the scalar field and provide the gradient information to the controller. The forward velocity is set as a constant gain. The output of the controller determines the next position of the mobile robot in the map $J(x,y)$.

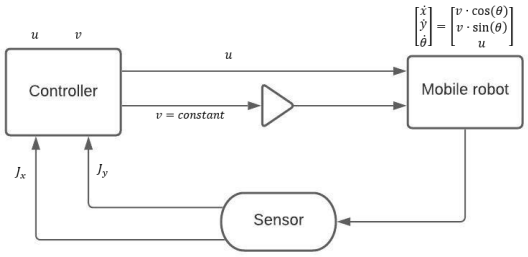

Figure 3: Control system of the mobile robot

B. *Kinematics*

This problem considers a non-holonomic system as the state of the mobile robot depends on its preceding path. The next state of the mobile robot depends on the intermediate value of the previous state. The scalar signal data is measured by the sensors that the robot carries.

The kinematic equation of the robot is given by,

$$\begin{bmatrix} \dot{x} \\ \dot{y} \\ \dot{\theta} \end{bmatrix} = \begin{bmatrix} v \cdot \cos(\theta) \\ v \cdot \sin(\theta) \\ u \end{bmatrix} \quad (4)$$

where x and y are the real-time position of the robot in the field, θ stands for the real-time heading angle and v is a velocity constant gain [12].

C. Gradient

As discussed in Section II.A, the gradient represents the increase or decrease and direction at a specific point in the scalar-valued field. The gradient ∇J at point $p = (x, y, \dots)$ can be defined as

$$\nabla J(p) = \begin{bmatrix} \frac{\partial f}{\partial x}(p) \\ \frac{\partial f}{\partial y}(p) \\ \vdots \end{bmatrix}. \quad (5)$$

The airflow field in this report is a 2 -dimensional signal field (x, y), therefore the gradient is a 2-dimensional vector and is specified as follows.

$$\nabla J(x, y) = \begin{bmatrix} \frac{\partial f}{\partial x}(x, y) \\ \frac{\partial f}{\partial y}(x, y) \end{bmatrix}. \quad (6)$$

The signal strength of the scalar-valued field is based on the shortest distance between point $p(x, y)$ and certain function. In the vector field, the gradient is represented by the white arrows in Figure 1 and 2. In order to increase the magnitude of the gradient as the distance increases between point p and the function, the squared scalar-valued field is taken.

The gradient descent algorithm is a method to find the local minimum of a differentiable function. If there is no slope, the local minimum is found. The gradient shows a zero vector. In the scalar-valued field of Figure 1 and 2, the local is reached when the distance between point p and function $f(x)$ or $f(y)$ is zero. The vector of the gradient from eq. (5) illustrates the direction in which scalar-value rises most. Accordingly, the minimum can be found by the performance of the opposite vector, given by $-\nabla J$.

The constant c_1 determines whether the aim is to find the local minimum or maximum. When $c < 0$ and $c > 0$, the constant holds for the gradient descent and gradient ascent, respectively [13].

$$\nabla J(x, y) = c_1 \begin{bmatrix} \frac{\partial f}{\partial x}(x, y) \\ \frac{\partial f}{\partial y}(x, y) \end{bmatrix}. \quad (7)$$

D. Orientation of the Robot

The orientation of the mobile robot is needed to obtain a proper control law design. The orientation of the robot can be compared to the local gradient information to gain the next real-time heading angle of the mobile robot. The orientation of the mobile robot is denoted by the normalized vector,

$$\vec{v} = \begin{bmatrix} \hat{x} \\ \hat{y} \end{bmatrix} = \begin{bmatrix} \cos(\theta) \\ \sin(\theta) \end{bmatrix} \quad (8)$$

E. Convex combination

A convex combination is a combination of points that are related to the specific point p. The output of the convex combination are non-negative weight factors and sum to 1.

The convex combination is needed when the mobile robot is not located at an integer point $p(x, y)$ in the signal field $J(x, y)$. At this non-integer specific point in the signal field, there is no information about the gradient. The controller combines the gradient information of the four points $((x_1, y_1), (x_2, y_2), (x_3, y_3), (x_4, y_4))$ that are the closest. Each of these points get a weight factor depending on the distance to point p related to the other three distances. The convex combination approximates the gradient at the mobile robot's real-time location. Consequently, the controller of the mobile robot is able to obtain gradient information at each real-time location.

Figure 4 shows a convex combination between four points and point p, the smaller d_n the greater the weight factor. All weight factor sum 1.

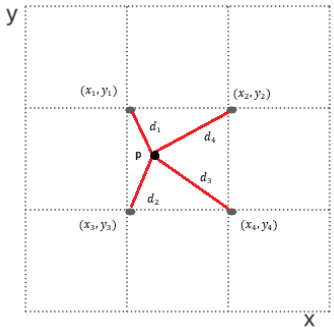

Figure 4: Convex combination between point p and its four closest point.

F. Control Law

Based on the theories elaborated in the previous parts, a control law for the angular velocity u is designed. Figure 5 denotes the orientation $\vec{v}$, the gradient $-\nabla J$ and the orthogonal gradient $\nabla J^{\perp}$ at some point in a signal field.

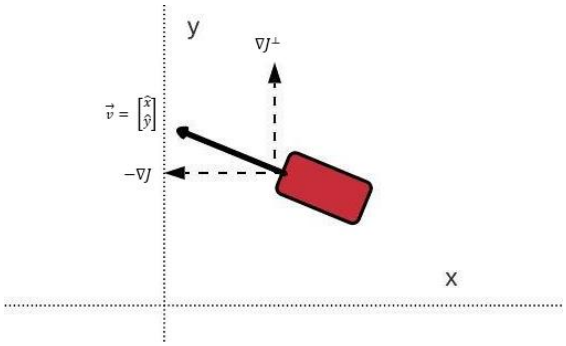

Figure 5: Orientation of the mobile robot and gradient

The vectors $\nabla J^{\perp}$ and ∇J are orthogonal if they are perpendicular (i.e. they form a right angle), the inner space product of the two vectors are equal to zero, the cross product is greater than zero and the magnitude of both vectors are equal to each other.

$$\nabla J(x, y)(\nabla J^{\perp}(x, y))^{\top} = 0, \quad (9)$$

$$\nabla J^{\perp}(x, y) \times \nabla J(x, y) > 0, \quad (10)$$

$$\|\nabla J^{\perp}(x,y)\| = \|\nabla J(x,y)\|. \quad (11)$$

Figure 5 shows that $\nabla J^{\perp}$ is 90° of ∇J.

In order to find the minimum change in gradient information, the orientation of the mobile robot is multiplied by the gradient at the real-time location. Consequently, the control law is specified as

$$u = K_1 \begin{bmatrix} \hat{x} \\ \hat{y} \end{bmatrix}^{\top} \nabla J \quad (12)$$

where K_1 is negative as the gradient descent algorithm is applied.

When the gradient is zero $(\nabla J = 0)$, the orthogonal gradient is equal to zero as well $(\nabla J^{\perp} = 0)$, the minimum is reached and the mobile robot keeps following the minimum with constant forward velocity v

If the mobile robot crosses the path of the local minimum, the direction of the gradient ∇J flips 180° and consequently the orthogonal gradient $\nabla J^{\perp}$ flips 180°. The angular velocity output is reversed now. To tackle this problem and keep the mobile robot on track, the $\text{sign}\left(\begin{bmatrix}1\\0\end{bmatrix}^{\top} \nabla J^{\perp}\right)$ is added to the control law. This part provide an output of 1 or -1. When the gradient information flips 180°, the output changes from 1 to -1 or vice versa. In this case, the mobile robot keeps steering to the right trajectory. Next, the magnitude of the gradient is added or subtracted to eq. (12) to ensure the mobile robot finds the global minimum of $J(x,y)$.

$$u = -K_1 \cdot \text{sign}\left(\begin{bmatrix}1\\0\end{bmatrix}^{\top} \nabla J^{\perp}\right) \cdot \begin{bmatrix} \hat{x} \\ \hat{y} \end{bmatrix}^{\top} \nabla J - K_2 \cdot \text{sign}\left(\begin{bmatrix}1\\0\end{bmatrix}^{\top} \nabla J^{\perp}\right) \cdot \|J_x\| \quad (13)$$

The control law from eq. (9) is tested during the simulation and further evaluated in Section IV.

IV. SIMULATION

In this section, the results of the simulation are presented. Monte Carlo simulations are used to execute the simulations. The simulations are needed to validate the designed control law and investigate whether the mobile robot will autonomously navigate itself along the path where the airflow is the lowest in the signal field. The Monte Carlo method rely on repeated random samplings to obtain numerical results [14]. The results of a Monte Carlo Simulation are more representative as the simulations are based on varying initial conditions [14]. The domain is determined first. Next, all simulation are executed by performing a deterministic computation on randomized generated inputs and the results are presented.

First, the initial conditions are described. Next, the trajectories of four arbitrary simulations in the signal fields are shown. The performance of the control law is evaluated by investigating the influence of K_1 and K_2 on error distance and the settling time. In this report, the effect on the rise time with different constant values is not considered, as the convergence rate to the global minimum in the signal field is linear. Therefore, the rise time highly depends on the randomized initial position of the mobile robot in the signal field. Accordingly, this data is not relevant. The constant values of K_1 and K_2 are set to 5, 10, 20. During all simulations the ratio of constants K_1, K_2 is equal to 1, as this ratio shows the best results regarding the trajectory of the robot (Appendix A). Next, the robustness of the control is tested by adding noise to the system. The accuracy of the gathered gradient information is set to 50%, 80% and 100%.

All simulations are performed N=50 times, where N is a randomly generated input within the domain of the signal field $J(x,y)$.

The results of the error distance and settling time are illustrated in boxplots. The explanation of the construction of a boxplot can be found in Appendix B.

A. *Initial conditions*

The simulations are performed in two different signal fields, where the scalar-valued signal field were defined as $J_1(x,y)$ and $J_2(x,y)$. The signal shows a minimum when point p lays on $f(y) = 0$ or $f(x) = 0.01x^3$.

The distribution of the scalar-valued signal field corresponding with the airflow velocities is presented in Figures 6 and 7.

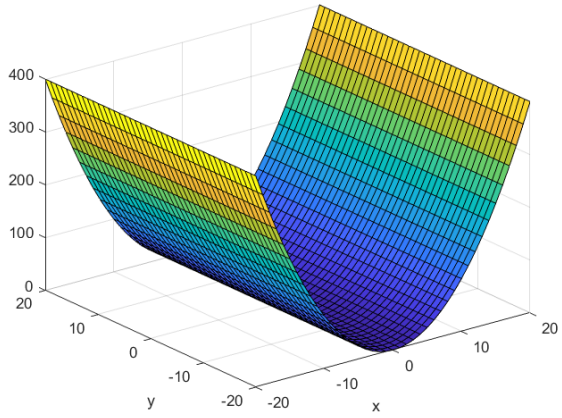

Figure 6: Surface plot of $J_1(x,y)$

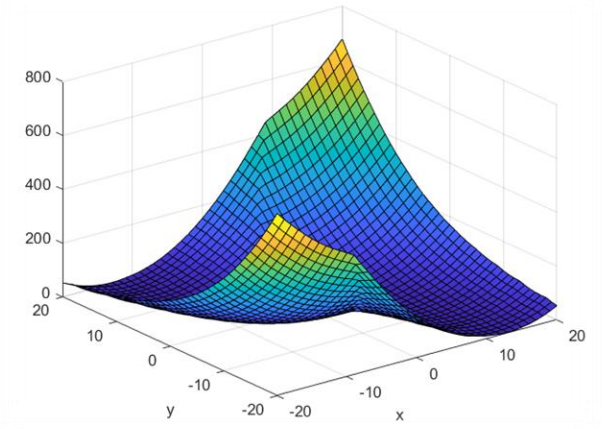

Figure 7: Surface plot of $J_2(x, y)$

As can be seen in the surface plot the domain for x and y is set as follows,

$$-20 \leq x \leq 20 \quad (14)$$

$$-20 \leq y \leq 20 \quad (15)$$

The initial condition for θ is specified as,

$$0 \leq \theta \leq 360 \quad (16)$$

B. *Trajectory of the mobile robot*

Figure 8 and 9 show the trajectory of the mobile robot from four arbitrary simulations in the two different scalar-valued signal fields. In all simulations time T set to 400 seconds with sampling time $T_s = 0.01$ s. The velocity constant is $v = 0.2$ m/s. The constants K_1 and K_2 are set to 10. It seems that the mobile robot steers itself to the local minimum. When the global minimum is reached, the mobile robot keeps following the trajectory of the line or curve shown in Figure 7 and 8, respectively.

In Figure 8, an overshoot appears when the global minimum is reached, this overshoot decrease as the time endures. The size of the overshoot depends on the value of K_1 and K_2, which is shown Section IV.C.

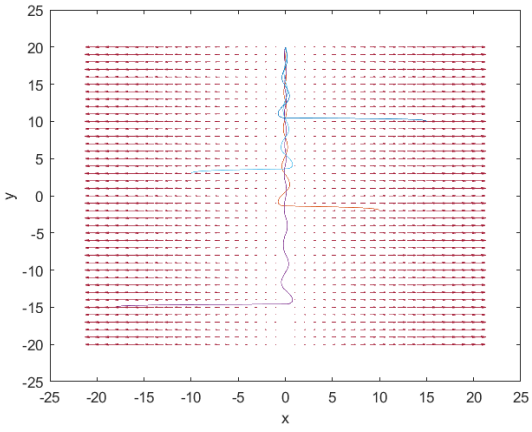

Figure 8: Four arbitrary simulations and the corresponding trajectory of the mobile robot, where K_1 and K_2 are 10.

The trajectory of the mobile robot in the scalar-valued signal field in which the curve $f(x) = 0.01x^3$ is set as minimum is presented in Figure 9. It seems that the mobile robot navigates to and keeps following the minimum path. However, it does not appear that the overshoot related to the curve decreases as the time increases. The overshoot does not decrease due to the fact that the gathered gradient information in this signal field does not match perfectly to the curve $f(x) = 0.01x^3$, which is the case in Figure 8 to line $f(y) = 0$. Consequently, the four arbitrary simulations show the same curly behaviour as the time endures.

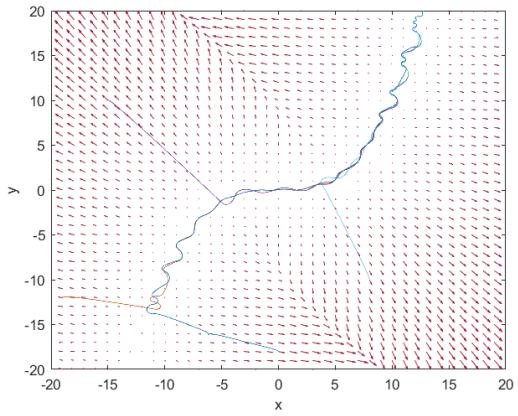

Figure 9: Four arbitrary simulations and the corresponding trajectory of the mobile robot, , where K_1 and K_2 are 10.

C. *Error distance*

The error distance is measured after $T = 100$ for three different constant values, where K_1 and K_2 are 5, 10 and 20, respectively. The results are shown in Figure 9 and 10.

In Figure 10, it appears that the error distance decreases if the constant values K_1 and K_2 increase. The boxplot of the error distance (Figure 10) is supported by the trajectory of the mobile robot with these different constant values which are revealed in Appendix C. The mobile robot shows better behaviour as K_1 and K_2 increase.

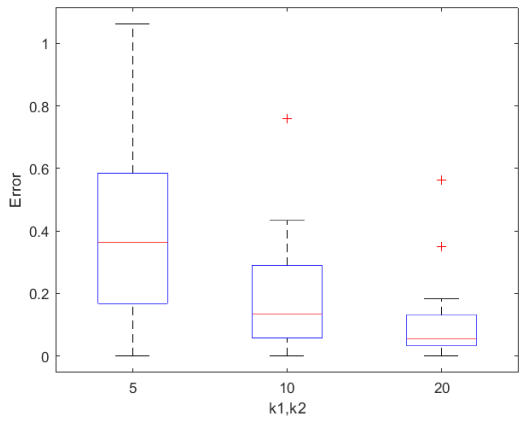

Figure 10: Error distance after $T = 100$ at signal field $J_1(x, y)$, where K_1 and K_2 are set to 5, 10 ,20.

The behaviour of the mobile robot in signal field $J_2(x, y)$ reveals no improvement as the constants K_1 and K_2 increase. The error distance stays roughly the same under the different conditions. Compared to signal field $J_1(x, y)$ the error distance in slightly larger when K_1 and K_2 are equal to 5. The error distance is significantly larger when K_1 and K_2 are set to 5 and 10. As discussed in Section IV.B, the gradient information in $J_2(x, y)$ is not as accurate as in $J_1(x, y)$. Therefore, the mobile robot does not converges to the minimum of $J_2(x, y)$ after certain time.

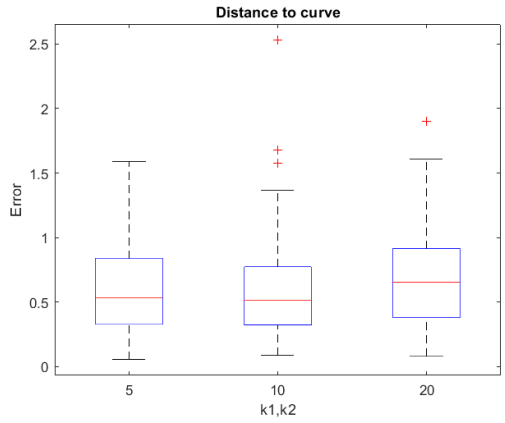

Figure 11: Error distance after $T = 100$ at signal field $J_2(x, y)$, where K_1 and K_2 are set to 5, 10 ,20.

D. Settling time

The settling time is equal to the time it takes the mobile robot to steer itself within 2% of the error distance of the desired state. The 2% error distance is related to the initial position of the mobile robot. Besides, the settling time is reached when the mobile robot stays within this 2% range. The settling time is evaluated in signal field $J_1(x, y)$ only as the gradient information and therefore the settling time results in $J_2(x, y)$ were inaccurate.

The settling time decreases as the K_1 and K_2 increase. The decrease of settling time along with the increase of K_1 and K_2 is justified by the trajectory of the mobile robot under these conditions (Appendix C). In the case that the mobile robot starts at the desire state, it steers itself along the minimum path and no settling time is noticed. The two outliers where the settling time T_s=0 can be explained by the fact that the mobile robot starts and stays at desired state.

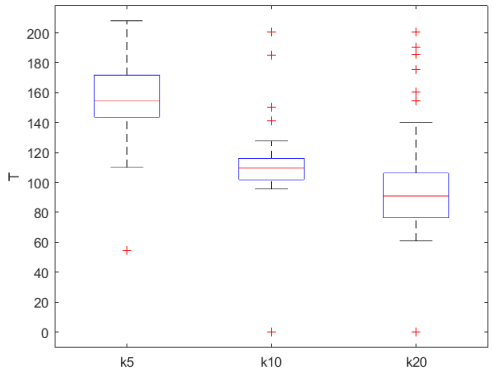

Figure 12: Settling time after $T = 100$ at signal field $J_1(x, y)$, where K_1 and K_2 are set to 5, 10 ,20.

E. Robustness

In this part, the robustness of the control law in the two different signal fields is tested. The robustness is tested when the sensor measurement of the gradient information is inaccurate. The goal is to test whether the control law is robust when there are uncertainties about the performance of the sensor measurement, which has directly impact on the gradient information. The sensor accuracy is set within three ranges: a weight factor of 0.5-1.5, a weight factor of 0.8-1.2 and a weight factor of 1.0 of the real gradient, which is the ideal circumstance, are added to the gradient ∇J. The constant value K_1 and K_2 are set at 10 during these simulations. Figure 12 reveals the error distance after $T = 100$ seconds, where the noise with their corresponding factors 0.5-1.5, 0.8-1.2, 1.0 is illustrated on the x-axis.

It appears that despite of the noise added to the sensor, the error distance stays stable. The steady error distance implies that the noise has minimal influence on the behaviour of the mobile robot regarding the error distance. The trajectories of four arbitrary simulations with a noise factor between 0.5-1.5 support the boxplot (Appendix D).

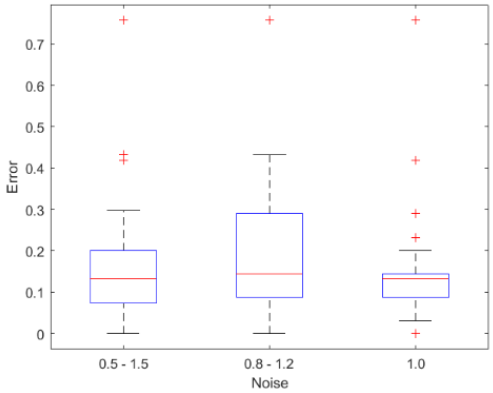

Figure 13: Error distance after $T = 100$ at signal field $J_1(x, y)$, where a noise weight factor is added; 0.5-1.5, 0.8-1.2, 1.0

The behaviour of the mobile robot with added noise in signal field $J_2(x, y)$ is illustrated in Figure 14. The error distance stays stable with different factors of noise added. Compared to the behaviour of the mobile robot in signal field $J_1(x, y)$, the error distance is greater in signal field $J_2(x, y)$. This difference in behaviour is in line with the obtained results in Section IV.C.

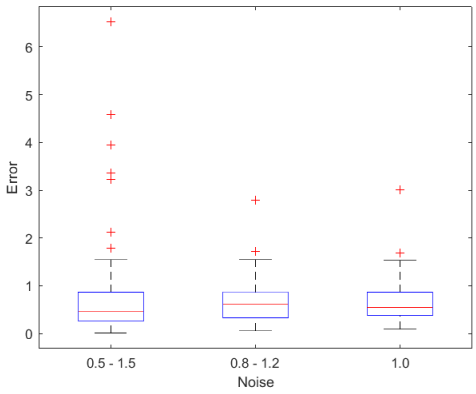

Figure 14: Error distance after $T = 100$ at signal field $J_2(x, y)$, where a noise weight factor is added; 0.5-1.5, 0.8-1.2, 1.0

V. DISCUSSION

Regarding the results of the simulations in Section IV, it can be stated that the mobile robot is able to find and follow the trajectory where the magnitude of the scalar value in the signal field is the lowest. The mobile robot shows decent behaviour in both signal fields. As discussed in Section IV, the behaviour of the mobile robot in the signal field $J_2(x, y)$ is slightly inaccurate. However, the inaccuracy is caused by the imprecise gradient measurements. Consequently, the designed control law show proper performances in both signal fields.

Next, the error distance is discussed. When the constant K_1 and K_2 increase the error distance decreases quicker over time. Therefore, the performance of the control law enhances as the constants K_1 and K_2 are raised from 5 to 20. During these simulations the results of the rise time appeared to be useless as the rise depended almost only on the initial position of the robot in the signal field. The boxplots regarding the settling time output provide a similar performance as the boxplots regarding the error distance simulated with varying values of K_1 and K_2.

The control law appears to be robust as the mobile robot is able to steer to the local minimum and keep following the minimum path when noise with different weight factor is added to the sensor measurements. In other words, the mobile robot is capable to navigate itself through an unknown environment along the desired trajectory when the sensor measurements are nonoptimal.

The designed control law shows potential and the mobile robot navigates itself as desired during the simulation. Although, the behaviour of the mobile robot is not tested in the real world. At that stage, real flow sensors are attached to the robot and these sensors might react undesirable. Despite of the robustness test during the simulations, the real flow sensor can behave different.

The goal is reached as the mobile robot behaves as the aim is set. Although, considering the higher goal of saving fuel consumption and reduces CO2 emissions, work has to be done. Analyzing this goal, the trajectory in Appendix A.2 shows possibilities in saving fuel for example. In this case, the path to the global minimum is longer, although the path to the top of the signal field at $J_1(0,20)$, which is a possible end point, is shorter. The shorter the path, the less fuel consumption. On the other hand, the aerodynamical drag needs to be taken in account along this path. The trajectories of the mobile robot in Figure 7 are not applicable yet to a real world situation. In this case, the aerodynamical drag is taken in account and the shortest path is not. In summary, the control law performance based on gradient information is accurate. On the other hand, aspects as shortest path are not taken in account considering the proposed control law.

VI. CONCLUSION

The proposed control law fulfills the condition that the mobile robot is capable to move around and find and follow the path with the minimum airflow in an unknown environment. The trajectories of the mobile robot appeared to be stable under different circumstances where different ratios and values of the constants K_1 and K_2 were tested and noise was added. Monte Carlo simulations were used to obtain a good overview of numerical results. Within the aim of this report, the ratio of 1:1 for constant values K_1 and K_2 is presented as optimal. Furthermore, the error distance and settling time decreases as the constant values K_1 and K_2 increases form 5 to 20. The results of the mobile robot in signal field $J_2(x, y)$ showed less stable results compared to the mobile robot performance in signal field $J_1(x, y)$ as the gradient information was inaccurate in $J_2(x, y)$ during the simulations. The gradient information is essential to ensure a proper performance of the mobile robot. During the simulations the gradient information was provided by a signal field. The control law showed potential when noise was added to the gradient information. In the real world, the gradient information is provided by flow sensor measurement, which can be tested and further investigated in future work.

VII. REFERENCES

[1] Schwab, K. and Davis, N., 2018. *Shaping the future of the fourth industrial revolution*. Currency.

[2] Russell, A., Thiel, D. and Mackay-Sim, A., 1994, May. Sensing odour trails for mobile robot navigation. In *Proceedings of the 1994 IEEE International Conference on Robotics and Automation* (pp. 2672-2677). IEEE.

[3] Cook, G. and Zhang, F., 2020. *Mobile Robots: Navigation, Control and Sensing, Surface Robots and AUVs*. John Wiley & Sons.

[4] Wobschall, D., Zeng, M. and Srinivasaraghavan, B., 2005, February. An ultrasonic/optical pulse sensor for precise distance measurements. In *2005 Sensors for Industry Conference* (pp. 31-34). IEEE.

[5] Liu, C., 2012. Foundations of MEMS. Pearson Education India

[6] Al Alam, A., Gattami, A. and Johansson, K.H., 2010. An experimental study on the fuel reduction potential of heavy duty vehicle latooning. In *13th International IEEE Conference on Intelligent Transportation Systems* (pp. 306-311). IEEE.

[7] Turri, V., Besselink, B. and Johansson, K.H., 2016. Cooperative look-ahead control for fuel-efficient and safe heavy-duty vehicle platooning. *IEEE Transactions on Control Systems Technology*, *25*(1), (pp.12-28). IEEE.

[8] Mährle, C., Wolff, S., Held, S. and Wachtmeister, G., 2019, October. Influence of the Cooling System and Road Topology on Heavy Duty Truck Platooning. In *2019 IEEE Intelligent Transportation Systems Conference (ITSC)* (pp. 1251-1256). IEEE.

[9] Barabash, O., Dakhno, N., Shevchenko, H. and Sobchuk, V., 2018, October. Integro-Differential Models of Decision Support Systems for Controlling Unmanned Aerial Vehicles on the Basis of Modified Gradient Method. In *2018 IEEE 5th International Conference on Methods and Systems of Navigation and Motion Control (MSNMC)* (pp. 94-97). IEE

[10] Kasac, J., Deur, J., Novakovic, B., Kolmanovsky, I.V. and Assadian, F., 2010. A conjugate gradient-based BPTT-like optimal control algorithm with vehicle dynamics control application. *IEEE Transactions on control systems technology*, *19*(6), (pp.1587-1595). IEEE.

[11] Soltero, D.E., Schwager, M. and Rus, D., 2014. Decentralized path planning for coverage tasks using gradient descent adaptive control. *The International Journal of Robotics Research*, *33*(3), (pp.401-425).

[12] Yang, J.M. and Kim, J.H., 1999. Sliding mode control for trajectory tracking of nonholonomic wheeled mobile robots. *IEEE Transactions on robotics and automation*, *15*(3), (pp.578-587). IEEE.

[13] Bachmayer, R. and Leonard, N.E., 2002, December. Vehicle networks for gradient descent in a sampled environment. In *Proceedings of the 41st IEEE Conference on Decision and Control, 2002.* (Vol. 1, pp. 112-117). IEEE.

[14] Kroese, D.P., Brereton, T., Taimre, T. and Botev, Z.I., 2014. Why the Monte Carlo method is so important today. *Wiley Interdisciplinary Reviews: Computational Statistics*, *6*(6), (pp.386-392)

IX. APPENDICES

A.

Appendix A shows the behaviour of the mobile robot after $T = 400$ when K_1 and K_2 are set to different ratios. The ratio 1:1 is considered as smoothest.

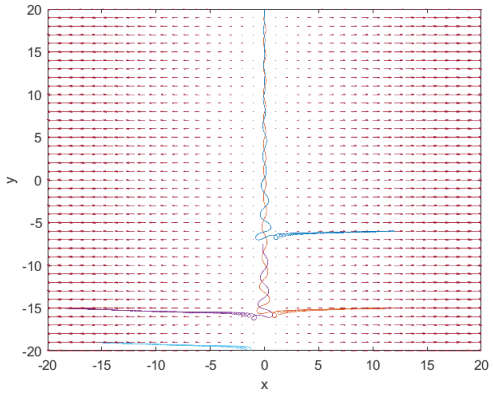

Appendix A.1: *Trajectory of four arbitrary simulations where K_1=10 and K_2= 20*

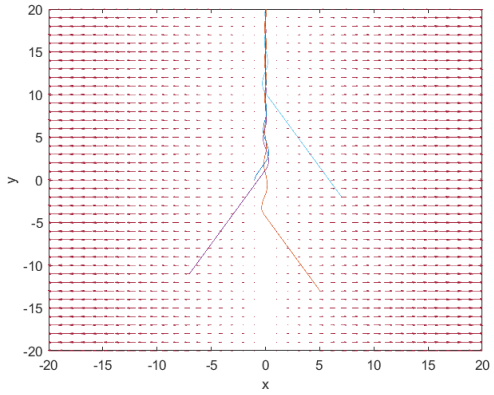

Appendix A.2: *Trajectory of four arbitrary simulations where K_1=20and K_2= 10*

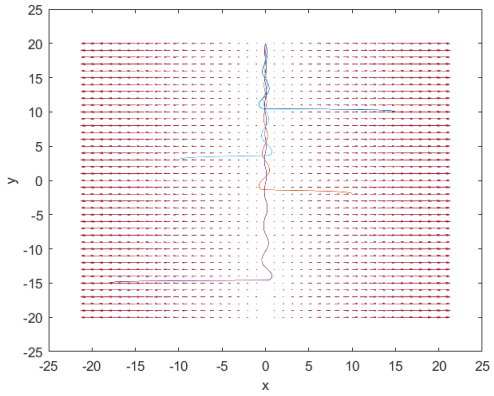

Appendix A.3: *Trajectory of four arbitrary simulations where K_1=10 and K_2= 10*

B.

The boxplots showed in this report are based on dataset with N=50 randomly generated initial inputs. The explanation of the construction of a boxplot is presented in Appendix B

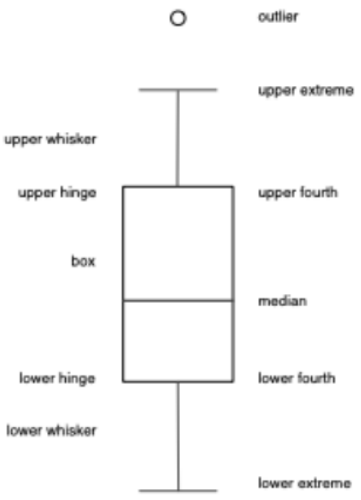

Appendix B: *Construction of a boxplot*

C.

Considering Appendix C, the magnitude of the constants $K_1$and K_2 has influence on the overshoot at the minimum in the signal field. The larger $K_1$and K_2, the smaller the overshoot. Consequently, along with the overshoot the error distance decreases.

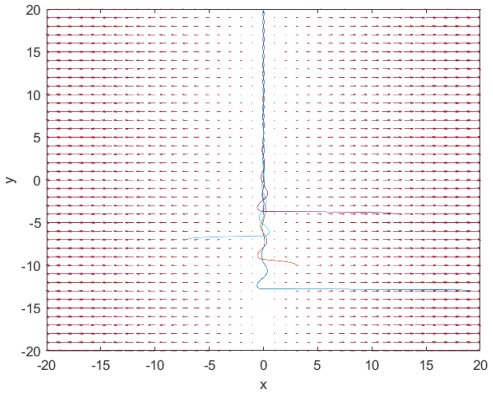

Appendix C.1: *Trajectory of four arbitrary simulations where K_1=20 and K_2= 20*

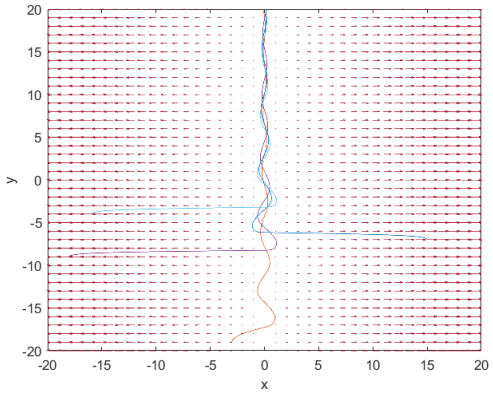

Appendix C.2: *Trajectory of four arbitrary simulations where K_1=5 and K_2= 5*

D.

Appendix D shows the behaviour of the mobile robot when noise is added to the sensor measurements. K_1 and K_2 are set to 10.

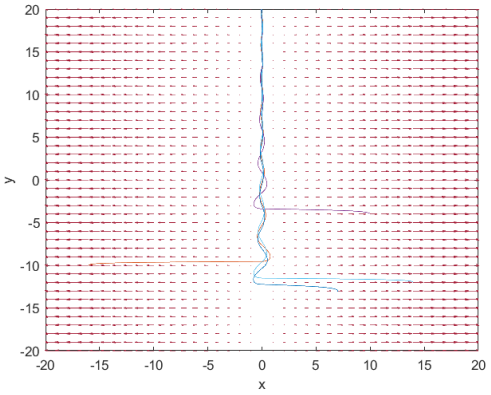

Appendix D.1: *Trajectory of four arbitrary simulations where a weight factor of 0.8-1.2 noise is added to the sensor measurements.*

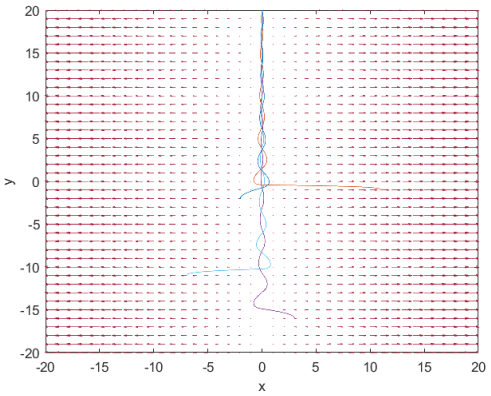

Appendix D.2: *Trajectory of four arbitrary simulations where a weight factor of 0.5-1.5 noise is added to the sensor measurements.*